The 2dF Galaxy Redshift Survey: a targeted study of catalogued clusters of galaxies

Roberto De Propris,[1]★ Warrick J. Couch,[1] Matthew Colless,[2] Gavin B. Dalton,[3]
Chris Collins,[4] Carlton M. Baugh,[5] Joss Bland-Hawthorn,[6] Terry Bridges,[6]
Russell Cannon,[6] Shaun Cole,[5] Nicholas Cross,[7] Kathryn Deeley,[1] Simon P. Driver,[7]
George Efstathiou,[8] Richard S. Ellis,[9] Carlos S. Frenk,[5] Karl Glazebrook,[10]
Carole Jackson,[2] Ofer Lahav,[11] Ian Lewis,[6] Stuart Lumsden,[12] Steve Maddox,[13]
Darren Madgwick,[8] Stephen Moody,[8,9] Peder Norberg,[5] John A. Peacock,[14]
Will Percival,[14] Bruce A. Peterson,[2] Will Sutherland[3] and Keith Taylor[9]

[1]*Department of Astrophysics, University of New South Wales, Sydney, NSW 2052, Australia*
[2]*Research School of Astronomy and Astrophysics, The Australian National University, Weston Creek, ACT 2611, Australia*
[3]*Department of Physics, Keble Road, Oxford OX1 3RH*
[4]*Astrophysics Research Institute, Liverpool John Moores University, Twelve Quays House, Birkenhead L14 1LD*
[5]*Department of Physics, South Road, Durham DH1 3LE*
[6]*Anglo-Australian Observatory, PO Box 296, Epping, NSW 2121, Australia*
[7]*School of Physics and Astronomy, North Haugh, St Andrews, Fife KY6 9SS*
[8]*Institute of Astronomy, University of Cambridge, Madingley Road, Cambridge CB3 0HA*
[9]*Department of Astronomy, Caltech, Pasadena, CA 91125, USA*
[10]*Department of Physics and Astronomy, Johns Hopkins University, Baltimore, MD 21218-2686, USA*
[11]*Racah Institute of Physics, The Hebrew University, Jerusalem, 91904, Israel*
[12]*Department of Physics, University of Leeds, Woodhouse Lane, Leeds LS2 9JT*
[13]*School of Physics and Astronomy, University of Nottingham, Nottingham NG7 2RD*
[14]*Institute for Astronomy, University of Edinburgh, Royal Observatory, Blackford Hill, Edinburgh EH9 3HJ*

ABSTRACT

We have carried out a study of known clusters within the 2dF Galaxy Redshift Survey (2dFGRS) observed areas and have identified 431 Abell, 173 APM and 343 EDCC clusters. Precise redshifts, velocity dispersions and new centroids have been measured for the majority of these objects, and this information is used to study the completeness of these catalogues, the level of contamination from foreground and background structures along the cluster's line of sight, the space density of the clusters as a function of redshift, and their velocity dispersion distributions. We find that the Abell and EDCC catalogues are contaminated at the level of about 10 per cent, whereas the APM catalogue suffers only 5 per cent contamination. If we use the original catalogue centroids, the level of contamination rises to approximately 15 per cent for the Abell and EDCC catalogues, showing that the presence of foreground and background groups may alter the richness of clusters in these catalogues. There is a deficiency of clusters at $z \sim 0.05$ that may correspond to a large underdensity in the Southern hemisphere. From the cumulative distribution of velocity dispersions for these clusters, we derive a space density of $\sigma > 1000 \, \mathrm{km \, s^{-1}}$ clusters of $3.6 \times 10^{-6} \, h^3 \, \mathrm{Mpc^{-3}}$. This result is used to constrain models for structure formation; our data favour low-density cosmologies, subject to the usual assumptions concerning the shape and normalization of the power spectrum.

Key words: astronomical data bases: miscellaneous – surveys – galaxies: clusters: general – galaxies: distances and redshifts – cosmology: observations.

★E-mail: propris@bat.phys.unsw.edu.au

1   INTRODUCTION

Rich clusters of galaxies are tracers of large-scale structure on the highest density scales, and therefore are important and conspicuous 'signposts' of its formation and evolution. While observational studies of the structure and dynamics of rich clusters have by practical necessity had to assume them to be isolated, spherically symmetric systems, recent massive *N*-body simulations of large-scale structure growth (e.g., the *VIRGO* consortium; Colberg et al. 1998) have shown a much more complex picture. Clusters are seen to be located at the intersections of the intricate pattern of sheets, filaments and voids that make up the galaxy distribution. They are formed through the episodic accretion of smaller groups and clusters via collimated infall along the filaments and walls (e.g. Dubinski 1998, and references therein). As a result of this process, the large-scale structure that surrounds the cluster gets imprinted upon it, both structurally (on smaller scales) and dynamically.

Testing the predictions of the theoretical work, observationally, has not been easy, since it requires large quantities of photometric and (in particular) spectroscopic data covering entire clusters and their surrounding regions. However, with the 2dF Galaxy Redshift Survey (2dFGRS) (Colless 1998; Maddox et al. 1998) – the largest survey of its kind to be undertaken – this problem can be addressed in a significant way. The large ($\sim 10^7 h^{-3} \, \mathrm{Mpc}^3$) and continuous volumes of space mapped by the survey, together with its close to one-in-one sampling of the galaxy population, will ensure that it includes a large and representative collection of rich clusters, each of which is well sampled spatially over the desired large regions. Ultimately, when the survey is complete, it will be used in itself to generate a new 3D-selected catalogue of rich clusters, using automated and objective detection algorithms.

The main purpose of this paper is to undertake a preliminary study of catalogued clusters using these data, and to take a first look at such issues as the reality of 2D-selected clusters such as those in the Abell catalogue, the incidence of serious projection effects and contamination by foreground and background systems, and the space density of clusters and its variation as a function of redshift, richness and cluster velocity dispersion. An additional by-product of the paper is to present new redshift and velocity dispersion measurements for the clusters, updating existing data in some cases and providing completely new data in others. This will be used as the basis catalogue for an analysis of composite cluster galaxy luminosity functions and their variation with cluster properties, spectrophotometric indices and their dependence on local density, the star formation rates of galaxies in clusters and their surroundings; the X-ray temperature – velocity dispersion relation, and a study of bulk rotation in clusters and other applications, which will be presented in separate papers. In addition, this study will help define the nature of Abell clusters in 3D space, so that objective cluster-finding algorithms (to be applied to the 2dF data base upon completion of the survey) may be tailored to recover this catalogue.

Our focus on the space density of clusters is motivated by the fact that the *abundance* of clusters provides a probe of the amplitude of the fluctuation power spectrum on characteristic scales of approximately $10 \, h^{-1} \, \mathrm{Mpc}$ – corresponding to the typical cluster mass of $\sim 5 \times 10^{14} \, h^{-1} \, \mathrm{M}_\odot$. Once the average density is determined, the cluster abundance can provide constraints on the shape of the power spectrum. A well-known example of this is the observation that the standard cold dark matter (CDM) model, normalized to match the cosmic microwave background anisotropies from the *COBE* experiment, predicts an abundance of clusters in excess by one order of magnitude over the observations.

The cluster mass function may therefore be exploited as a cosmological test; however, determination of cluster masses is generally difficult. For this reason, the distribution of velocity dispersions has often been used as a surrogate (e.g. Crone & Geller 1995). In particular, the more massive, higher velocity dispersion clusters are less likely to suffer from biases and incompleteness, and their space density may provide constraints on models for the formation of large-scale structure. Previous work indicates that clusters with $\sigma > 1000 \, \mathrm{km \, s}^{-1}$ are relatively rare (e.g. Mazure et al. 1996, and references therein). Depending on the normalization and shape of the fluctuation spectrum, this can be used to constrain cosmological parameters. In most common models, the rarity of these objects is taken to imply a low value of the matter density.

The plan of the paper is as follows. In Section 2 we give a brief overview of the 2dFGRS observations. Section 3 then describes the selection of clusters for this study, and how the members in each were identified using the 2dFGRS data; we derive redshifts and velocity dispersions for a sample of objects with adequate data. In Section 4 we address the issues of contamination of the cluster catalogues and selection of appropriate samples for comparison with theoretical models. This is followed in Section 5 by a determination of the space density of the different sets of catalogued clusters studied here, and then in Section 6 we analyse this quantity as a function of cluster velocity dispersion, comparing it with cosmological models. Finally, a summary of our results is given in Section 7. A cosmology with $H_0 = 100 \, h \, \mathrm{km \, s}^{-1} \, \mathrm{Mpc}^{-1}$ and $\Omega_0 = 1$ is adopted throughout this paper.

2   OBSERVATIONS

The observational parameters of the 2dFGRS are described in detail elsewhere (Colless et al. 2001), and so only a brief summary is given here. The primary goal of the 2dFGRS is to obtain redshifts for a sample of 250 000 galaxies contained within two continuous strips (one in the northern and the other in the southern Galactic cap regions) and 100 random fields, totalling $\sim 2000 \, \mathrm{deg}^2$ in area, down to an extinction-corrected magnitude limit of $b_J = 19.45$. The input catalogue for the survey is based on the APM catalogue published by Maddox et al. (1990a,b), with modifications as described by Maddox et al. (in preparation).

Observations are carried out at the 3.9-m Anglo-Australian Telescope (AAT), using the Two-degree Field (2dF) spectrograph, a fibre-fed instrument capable of obtaining spectra for 400 objects simultaneously over a two-degree field (diameter). The instrument is described by Lewis et al. (in preparation). For the 2dFGRS, $300 \, \mathrm{line \, mm}^{-1}$ gratings blazed in the blue are used, yielding a resolution of $\sim 9 \, \text{Å}$ FWHM and a wavelength range of 3500–$7500 \, \text{Å}$. To date, the observing efficiency, accounting for weather losses and instrument down-time, has averaged ~ 50 per cent, with the overall redshift completeness running at ~ 95 per cent, based on a typical exposure time (per field) of $3600 \, \mathrm{s}$. The spectra are all pipeline-reduced at the telescope, with redshifts being measured using a cross-correlation method and subject to visual verification in which a quality index Q, which ranges between 1 (unreliable) and 5 (of highest quality), is assigned to each measurement. As of 2001 July, we had collected 195 497 unique redshifts, including 173 084 galaxies with good-quality spectra (the sample used here). The balance of objects consists of galaxies with poor spectra and stars misclassified as galaxies.

Table 1. 2dF Cluster Catalogue. The full version of this table is available in *Synergy*, the on-line version of Monthly Notices.

Cluster ID	APM #	EDCC #	RA (1950)	Dec (1950)	Previous *cz*	2dF *cz*	Error	σ	error (+ve)	error (-ve)	Number	Completeness	Notes
Abell 0015	030	419	00:12:46.96	−26:19:38.2	37204	36035	149	497	167	115	11	0.54	
Abell 0118	...	495	00:52:32.38	−26:38:45.9	34416	34283	157	725	160	117	23	0.58	
Abell 0157	...	...	01:08:45.20	−14:44:28.5	30999	31167	...	392	...	...	9	...	1
Abell 0159	...	...	01:09:30.00	−15:22:00.0	...	...	...	...	...	...	−	...	1
Abell 0176	...	...	01:17:04.46	−08:24:39.2	...	41317	...	304	...	...	9	...	1
Abell 0206	...	562	01:26:07.79	−25:52:48.8	...	61876	...	553	...	...	6	0.56	
Abell 0210	...	569	01:29:52.03	−26:15:38.2	...	40638	213	854	226	155	17	0.82	
Abell 0214	...	...	01:32:19.25	−26:22:29.0	...	40140	...	449	...	...	9	0.82	2
Abell 0214	...	576	01:32:02.54	−26:21:39.7	47877	48019	...	629	...	...	8	0.82	
Abell 0264	...	598	01:49:35.05	−26:02:11.8	43170	41997	94	303	117	98	15	0.73	
Abell 0297	...	613	01:59:48.73	−25:50:34.4	...	60049	...	1310	...	...	8	0.60	
Abell 0325	...	634	02:13:08.56	−25:18:10.5	...	...	...	...	...	...	−	0.29	
Abell 0327	...	633	02:10:37.13	−26:22:38.1	...	51025	...	424	...	...	6	0.61	
Abell 0368	...	673	02:35:12.00	−26:43:00.0	...	...	...	...	...	...	−	0.79	
Abell 0389	305	699	02:49:12.12	−25:08:57.7	33966	34085	118	667	90	115	35	0.55	
Abell 0419	...	729	03:06:03.57	−23:52:55.4	19846	21021	182	1147	136	173	41	0.28	3,4
Abell 0890	...	...	09:50:30.00	−04:36:00.0	...	...	...	...	...	...	−	0.95	
Abell 0892	...	...	09:51:03.68	+00:49:29.1	...	28038	217	1067	218	160	25	0.56	
Abell 0912	...	...	09:58:35.77	+00:09:40.7	13371	13744	77	354	84	70	28	0.59	
Abell 0919	...	...	10:02:19.64	−00:26:02.8	28600	28770	...	169	...	...	9	0.51	
Abell 0930	...	...	10:04:30.65	−05:22:48.4	16459	17316	97	907	76	88	91	0.84	
Abell 0933	...	...	10:05:14.50	+00:45:25.7	28660	29180	64	420	55	63	53	0.54	
Abell 0944	...	...	10:08:36.00	−01:47:00.0	...	...	...	...	...	...	−	0.68	
Abell 0954	...	...	10:11:11.10	+00:07:40.2	27941	28622	122	832	94	115	49	0.72	
Abell 0957	...	...	10:11:05.10	−00:40:38.9	13491	13623	79	722	63	73	88	0.71	
Abell 0978	...	...	10:17:56.11	−06:16:30.6	16309	16149	154	791	153	116	28	0.33	
Abell 0993	...	...	10:18:51.87	−04:35:13.3	...	11864	41	242	71	73	59	0.81	2
Abell 0993	...	...	10:19:24.36	−04:38:17.0	14630	16311	56	481	46	53	88	0.81	4
Abell 1008	...	...	10:22:12.00	−05:06:00.0	...	...	...	...	...	...	−	0.81	
Abell 1009	...	...	10:22:24.00	−05:32:00.0	...	...	...	...	...	...	−	0.72	
Abell 1013	...	...	10:23:24.00	−05:58:00.0	...	...	...	...	...	...	−	0.48	
Abell 1038	...	...	10:30:22.60	+02:30:13.0	37204	38238	116	329	144	110	11	0.79	
Abell 1039	...	...	10:30:18.07	−04:32:04.2	...	47592	...	...	...	...	1	0.88	5
Abell 1059	...	...	10:34:16.60	−05:45:53.5	...	48171	122	390	140	103	13	0.50	
Abell 1064	...	...	10:36:02.21	+01:33:25.5	39033	39530	117	550	119	91	25	0.83	
Abell 1078	...	...	10:41:03.18	+00:52:30.0	...	37276	123	527	128	96	21	0.84	6
Abell 1080	...	...	10:41:17.77	+01:19:30.4	...	35335	101	678	78	96	49	0.82	

1: in a random field; 2: foreground group; 3: Wegner et al. (1999) claim two groups; 4: redshift discrepant; 5: bright E galaxy at this position: cluster centre ?; 6: bright star 'hole' in APM catalog; 7: background group; 8: Mazure et al. (1996) claim a third group; 9: Mazure et al. claim a low redshift group and a higher redshift group; 10: Lumsden et al. (1992) have a different redshift; 11: Katgert et al. (1996) claim multiple systems; 12: merged with 3094 ?; 13: confused with S1043 ?; 14: confused with 4038 ?; 15: possibly embedded in larger structure; 16: same as edcc 061 ?; 17: same as edcc 176 ?; 18: same as A2923 ?.

3   CLUSTER SELECTION AND DETECTION

3.1   The cluster catalogues

Clusters for our study were sourced from the catalogues of Abell (Abell 1958; Abell, Corwin & Olowin 1989, hereafter ACO), the APM (Dalton et al. 1997) and EDCC (Lumsden et al. 1992).

Abell and collaborators selected clusters from visual scans of Palomar Observatory Sky Survey red plates and from SERC-J plates. For each cluster, a counting radius was assigned, equivalent to $1.5\,h^{-1}$ Mpc (the Abell radius), adopting a redshift based on the magnitude of the 10th brightest galaxy (m_{10}). The number of cluster galaxies between m_3 and $m_3 + 2$, where m_3 is the magnitude of the third brightest galaxy, was then used to assign a richness parameter, after subtracting an estimate for background and foreground contamination. Abell (1958) used a local background from areas of each plate with no obvious clusters, whereas ACO employed a universal background derived from integration of the local luminosity function.

Both the APM and EDCC use machine-based, magnitude-limited galaxy catalogues from the UK Schmidt plates. A full description of the APM selection algorithm is given by Dalton et al. (1997). The APM cluster survey used an optimized variant of Abell's selection algorithm that uses a smaller radius to identify clusters, and a richness estimate that is coupled to the apparent distance to compensate for the effects described by Scott (1956). This produces richness and distance estimates for the APM clusters, which are found to be robust, and which give well-defined estimates of the completeness limits for the catalogue. The large-scale properties of the final 2D catalogue are found to be consistent with the observed 3D distribution (Dalton et al. 1992).

Lumsden et al. (1992) adopt an approach similar to Abell; they bin their data in cells and lightly smooth the distribution to identify peaks, using a procedure akin to that of Shectman (1985). EDCC clusters are then related to the Abell catalogue, with the catalogue listing a richness class and magnitudes for the first-, third- and tenth-ranked galaxies.

By the nature of its visual selection, the Abell catalogue is somewhat subjective, and prone to contamination from plate-to-plate variations and chance superpositions. Lucey (1983) and Katgert et al. (1996) estimate that about 10 per cent of the clusters with richness class $R \geq 1$ suffer from contamination, whereas Sutherland (1988) argues for a 15–30 per cent level of contamination over the entire sample, including the poorer clusters. Here contamination is defined as the presence of foreground or background structure that substantially boosts the apparent richness of the system, in some cases allowing the
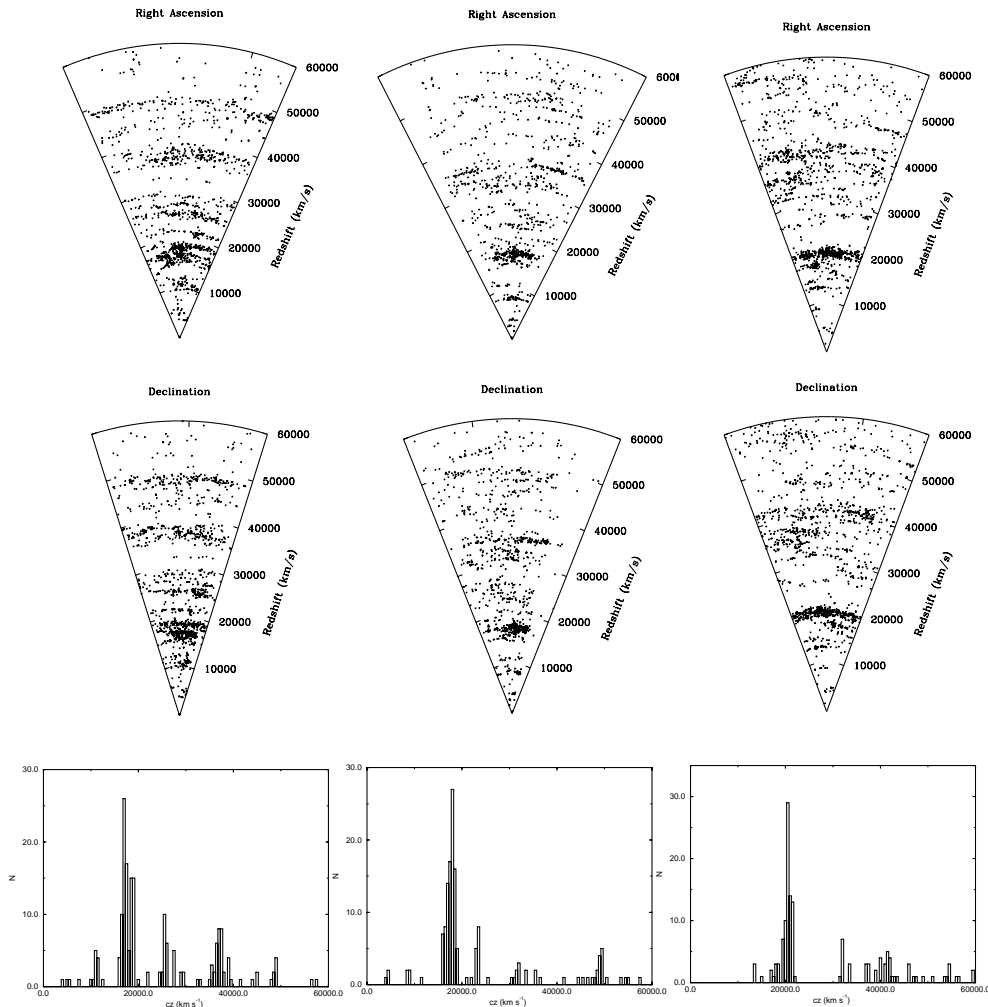

Figure 1. Cone diagrams and redshift histograms for the fields centred on Abell 0930, 3880 and S0333 (from left). The aperture is a circular one with radius corresponding to 6 Mpc at the cluster redshift.

inclusion in the catalogue of objects that would not satisfy the minimum richness criterion. This definition is, of course, somewhat arbitrary and subjective; we adopt a somewhat more quantitative definition when we examine the issue of contamination later in the paper. Sutherland & Efstathiou (1991) also infer the presence of significant spurious clustering in the Abell catalogues due to completeness variations between plates, although they do not quantify this further.

Both the APM and the EDCC claim to be more complete than the Abell catalogue, especially for poor clusters, and to be less affected by superposition and contamination. The EDCC claims to be complete for all clusters within the context of the stated selection criteria; it is built to imitate the Abell catalogue, and a comparison shows that about 50 per cent of the clusters are in common between the two catalogues. The APM uses a smaller counting radius than Abell and is claimed to be more complete for poorer clusters and to be more objectively selected (Dalton et al. 1997).

3.2 Cluster identification and measurement

We searched the 2dFGRS catalogue for clusters whose centroid, as given in the above catalogues, lay within 1 deg of the centre of one of the observed survey tiles. In doing so, our policy was to consider *all* clusters in each of the three catalogues without any pre-selection based on richness or distance class or any other property. The Abell catalogue is, in theory, limited to clusters with $z < 0.2$; however, it includes clusters with estimated redshifts that are substantially higher (e.g., Abell 2444 in the sample being considered here). Although these objects may well be too distant for 2dFGRS to detect, they are included in our tables none the less, since it is generally difficult to estimate cluster redshifts a priori.

If the centroid of a catalogued cluster was found in one of the 2dFGRS tiles, we then searched the 2dFGRS redshift catalogue for objects within a specified search radius of the cluster centroid. The search radius used was that particular to the catalogue from which the cluster originated. This isolates a cone in redshift space containing putative cluster members along with foreground and background galaxies. We then inspected the Palomar Observatory Sky Survey (POSS) plates for the brightest cluster galaxy: in most cases this was a typical central cluster elliptical with optical morphology consistent with a brightest cluster galaxy, and could therefore be easily identified as the cluster centre. Where this was not possible, in some clusters, we adopted the brightest cluster member with an image consistent with early-type morphology. We repeated our search procedure to produce more accurate lists of candidate members.

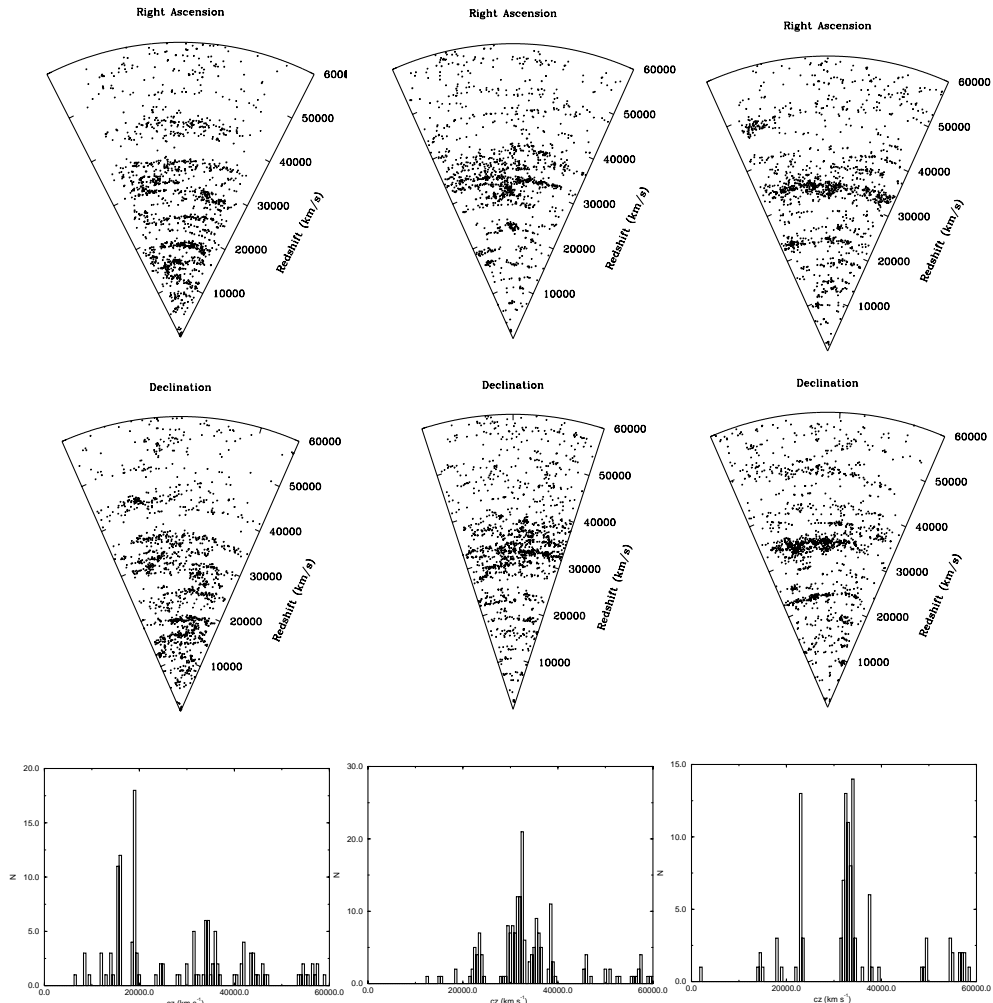An important consideration in this context is the adaptive tiling

Figure 2. Cone diagrams and redshift histograms for the fields centred on Abell 1308, 2778 and S0084.

strategy used in 2dF observations (Colless et al. 2001). Here, complete coverage of the survey regions is achieved through a variable overlapping (in the Right Ascension direction) of the 2dF tiles. In the direction of rich clusters where the surface density of galaxies is high, more overlap is clearly required. Hence we have to tolerate some level of incompleteness in the peripheries of our fields at this stage of the survey; this is a *temporary* situation, the implications of which will be discussed later in this section. In Table 1 we quote the completeness, viz. the fraction of 2dFGRS input catalogue objects within our search radius whose redshifts have been measured for each cluster field.

3.3 Cone diagrams

This transformation of the projected 2D distribution of galaxies upon the sky (on which the identification of a cluster was based) into a 3D one, presented us with three general cases as far as cluster visibility was concerned. (i) The cluster was easily recognizable as a distinct and concentrated collection of galaxies along the line of sight, with no ambiguity at all in its identification. Cone diagrams for three such examples (A0930, A3880 and S0333) are shown in Fig. 1. (ii) Several concentrations of galaxies were found along the line of sight. Where one was particularly dominant, the cluster identification was generally unambiguous, but foreground and background contamination was clearly significant. Two such

examples (A1308 and A2778) are shown in Fig. 2. If the different concentrations were of similar richness, then cluster identification became ambiguous and required further analysis via our redshift histograms (see below). An example of such a case (S0084) is also shown in Fig. 2. (iii) There were no clearly defined concentrations of galaxies at all within the cone, and the cluster, at this stage, could not be identified. Three such examples (A2794, A2919 and S1129) are shown in Fig. 3, where the 'cluster' appears in redshift space to be a collection of unrelated structures. Note that the opening angles of the cone diagrams are far larger than the search radius, corresponding to a metric radius of 6 Mpc for the adopted cosmology; this is done in order to show both the cluster and its surrounding large-scale structure. In contrast, the redshift histograms that we now discuss have been constructed from objects just within the search radius, in order to facilitate identification of the cluster peak.

To consolidate and quantify our cluster identifications, redshift histograms of the galaxies within the Abell radius were constructed and examined. These are also included in Figs 1–3 for each of the cone diagrams that are plotted. For the ambiguous case (ii) types, where the redshift histogram contained multiple and no singly dominant peaks (see A2778 in Fig. 2), the peak closest to the estimated redshift of the cluster was taken to be our identification. In none of the case (iii) situations did the redshift distribution allow us to identify a significant peak. All peaks that were found in the
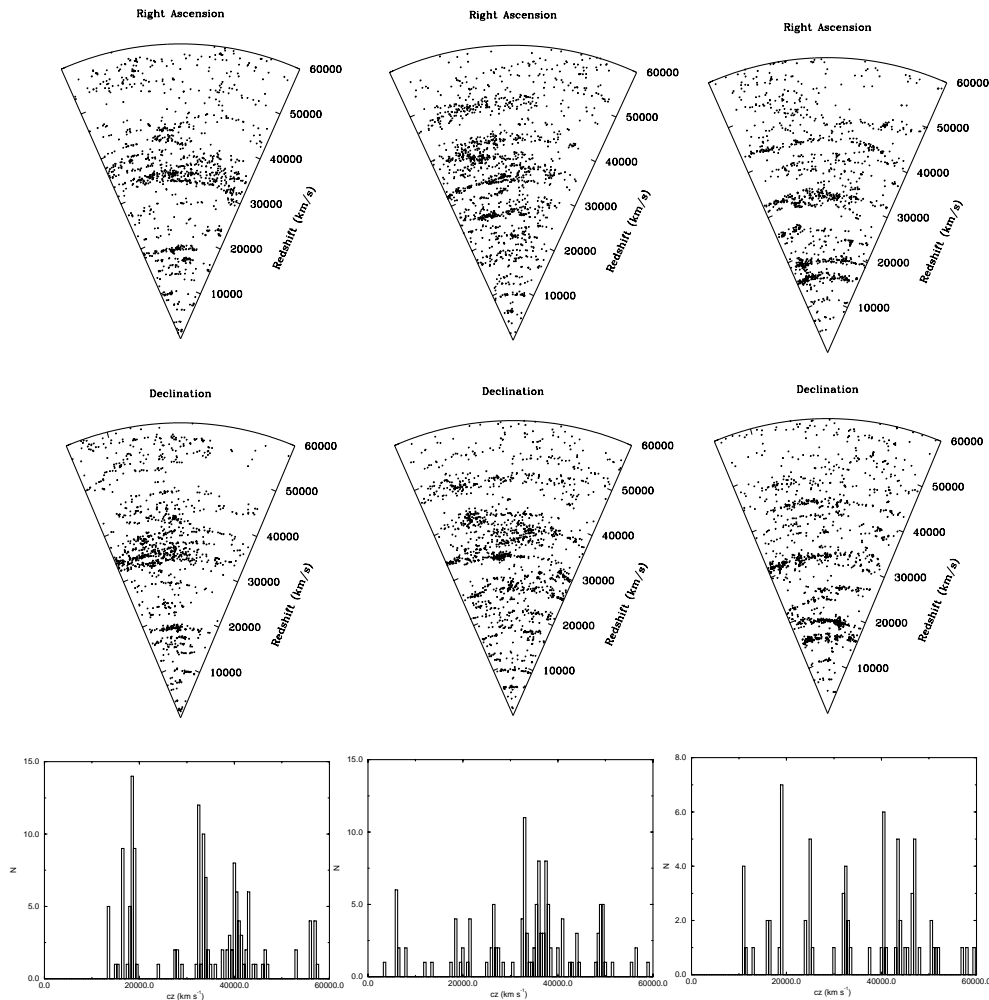

Figure 3. Cone diagrams and redshift histograms for the fields centred on Abell 2794, 2919 and S1129.

direction of each cluster are listed in Table 1. Notes indicate the presence of fore/background systems.

3.4 Redshifts and velocity dispersions

Mean redshifts and velocity dispersions were calculated from the redshift distributions, not only for the identified clusters but also for all the other significant peaks seen. In doing so, we followed the approach of Zabludoff, Huchra & Geller (1990, hereafter ZHG) to identify and isolate cluster members. The basis of this method is that (as shown in the redshift histograms in Figs 1–3) the contrast between the clusters and the fore/background galaxies is quite sharp. Therefore, physical systems can be identified on the basis of compactness or isolation in redshift space, i.e., on the gaps between the systems: in this latter case, if two adjacent galaxies in the velocity distribution are to belong to the same group, their velocity difference should not exceed a certain value, the *velocity gap*. ZHG use a two-step scheme along these lines, in which first a fixed gap is applied to define the main system, and then a gap equal to the velocity dispersion of the system is applied to eliminate outlying galaxies. The choice of the initial gap depends somewhat on the sampling of the redshift survey: e.g., ZHG use a $2000\,\mathrm{km\,s^{-1}}$ gap. In order to avoid merging well-separated systems into larger units (as we are better sampled than ZHG), we adopt a $1000\,\mathrm{km\,s^{-1}}$ gap. The choice of $1000\,\mathrm{km\,s}$ was found to be optimum in that it (i) avoids merging sub-cluster systems into a large and spurious single system, and (ii) is large enough to avoid fracturing real systems into many smaller groups. We also note that the value of $1000\,\mathrm{km\,s}$ that was used, is consistent with previous work and such a value is borne out by the distribution of velocity separations in the cluster line of sight pencil beams (cf., Katgert et al. 1996) and is operationally simpler than implementing a friends-of-friends algorithm. In principle this choice may introduce a bias with redshift, as the luminosity functions are less well sampled for more distant clusters, and this is the reason why most of our analysis below is carried out on the nearer portion of the sample.

The redshift bounds of the 'peak' corresponding to the cluster were set by proceeding out into the tails on each side of the peak centre until a velocity separation between individual galaxies of more than $1000\,\mathrm{km\,s^{-1}}$ was encountered. In other words, we define the cluster peak as the set of objects confined by a $1000\,\mathrm{km\,s^{-1}}$ void on either side in velocity space. The peak can have any width in velocity space, but is required to be isolated in redshift space. We then calculated a mean redshift and velocity dispersion for the galaxies in the peak, and ranked them in order of redshift separation from the mean value. We next identified the first object on either side of the mean whose separation in velocity from its neighbour (closest to the mean) exceeded the velocity dispersion, and then excised all objects further out in the wings of the distribution. The mean redshift and velocity dispersion were then recalculated following the prescription of Danese, de Zotti & di Tullio (1980), which provide a rigorous method to estimate mean redshifts, velocity dispersions and their errors based on the assumption that galaxy velocities are distributed according to a Gaussian.

If the final, excised sample contained fewer than 10 objects, a velocity dispersion was not calculated, since values based on such small numbers are too unreliable (Girardi et al. 1993). We quote the standard deviation of the mean in place of the velocity dispersion, but make no use of it in our analysis. These clusters are, however, included in our tables below, and in our analysis of completeness and the space density of clusters presented in the following

sections. By imposing this number threshold, we should also decrease our sensitivity to sampling variations (due to the increased fibre collisions in denser fields and therefore lower completeness for cluster fields).

This procedure is a simplified form of the 'gapping' algorithm suggested by Beers, Flynn & Gebhardt (1990). Previous work has generally employed the pessimistic 3σ clipping technique of Yahil & Vidal (1977). One advantage is that the ZHG technique does not assume a Gaussian distribution of velocities and discriminates against closely spaced peaks, corresponding to a lower σ clip in the case of a pure normal distribution. On the other hand, the 3σ clipping method is more effective at removing spurious high-velocity-dispersion objects when the fields are sparsely sampled. A comparison between the two methods has been carried out by Zabludoff et al. (1993): while the results are usually consistent within the 1σ error, there is a tendency for 3σ clipping to yield somewhat lower velocity dispersions.

3.5 The cluster tables

Table 1 lists all unique clusters detected (where unique means detected in a single catalogue, avoiding counting objects more than once if they are present in more than one catalogue: the order of preference is Abell, APM and EDCC). This includes 1149 objects (including double or triple systems where more than one identifiable cluster or group is present in the line of sight) and 753 single clusters (i.e., assuming that only one of the eventual multiple systems corresponds to the catalogued cluster). Of these, 413 are in the Abell/ACO catalogues, 173 in APMCC and 343 in EDCC. The structure of the table is as follows: column 1 is the identification, columns 2 and 3 are cross-identifications in other catalogues, columns 4 and 5 are the RA and Dec. of the cluster centroid (see above), column 6 is the redshift we derive along with its error, column 7 is the velocity dispersion, column 8 is the number of cluster members, and column 9 is the redshift completeness (expressed as a percentage) in the 2-deg (diameter) tile where the cluster is located. Column 10 contains essential notes. Literature data are from the recent compilations of Collins et al. (1995), Dalton et al. (1997) and Struble & Rood (1999), unless otherwise noted. The first few lines of the table are printed here: the entire table is available in ASCII format from `http://bat.phys.unsw.edu.au/~propris/clutab.txt`

Having assembled the cluster redshifts, measured both here using the 2dFGRS data and previously by other workers, we can compare the two to provide an external check on our new 2dFGRS values. We compare redshifts for clusters which have more than six measured members in 2dFGRS. To avoid confusion, we consider only clusters with a single prominent peak, since in the cases where more than one structure is present in the beam, the identification with the cluster is ambiguous. This comparison is shown graphically in Fig. 4 where we see a good one-to-one relationship between the two. Formally, we find a mean difference between our redshift measurements and other measurements of $\Delta cz = 89 \pm 307\,\mathrm{km\,s^{-1}}$. This excludes a small number of objects where the 2dF and literature redshift disagree by large values: such cases appear to occur when the cluster centroid in the original catalogue is misidentified, or when only one or two galaxies are used to derive the previously published redshift.

Finally, in Table 2 we summarize the total numbers of clusters from each catalogue found within the 2dFGRS. It is important to stress that the sum of these totals does not represent the number of unique clusters that are studied here, since there is some overlap
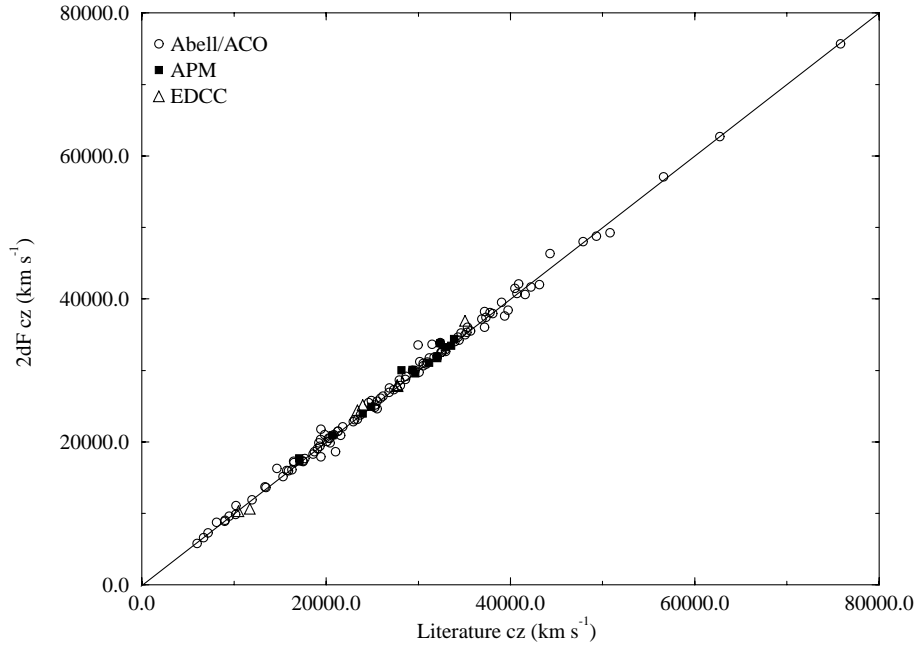
Figure 4. Comparison between literature and 2dF cluster redshifts.

Table 2. Summary of cluster identifications.

Catalogue	N(clusters)	N(Redshifts)	$N(\sigma)$
Abell	413 (42 APM, 133 EDCC)	263	208
APM	173 (42 Abell, 50 EDCC)	84	75
EDCC	343 (133 Abell, 50 APM)	224	174

between the three cluster catalogues (although we have analysed them separately according to the definitions of each catalogue – see above). We show the level of overlap by listing alongside the totals for each catalogue – in column 2 of Table 2 – the numbers of these clusters that are also found in the other two catalogues.

About one-third (32 per cent) of all Abell clusters are identified with an EDCC cluster, and 10 per cent with an APM cluster. Conversely, 24 per cent of APM clusters have an Abell counterpart, and 29 per cent an EDCC counterpart. For EDCC, 39 per cent of clusters are also identified in the Abell catalogue, and 15 per cent in the APM catalogue. Note that this comparison is confined to just the southern strip and does not include any of the clusters in the original Abell (1958) catalogue.

4 CLUSTER COMPLETENESS AND CONTAMINATION

Important to any quantitative analysis based on the clusters found here is the need to identify volume-limited subsamples, underpinned by a good understanding of the completeness of the input cluster catalogues and how the derived velocity dispersions maybe biased with redshift and cluster richness. We note in this regard that a properly selected 3D sample will be derived using automated group-finding algorithms once the survey has reached its full complement of galaxies and the window function is more regular.

In order to derive estimates of completeness and contamination, and to normalize the space density of clusters to determine the distribution of velocity dispersions (Section 5 below), we need to define properly volume-limited samples and correct our observations for incompleteness deriving from the adopted window function and detection efficiency. Here we adopt two routes: the standard approach has been to define 'cuts' in estimated redshift space to derive a (roughly) volume-limited sample, adopting a richness limit to ensure that the sample will be reasonably complete. We first comment on the accuracy of estimated redshifts and any empirical relation that exists between estimated and true (2dFGRS) redshift; afterwards we use this relation and our redshifts together to determine an estimate for the space density of clusters and choose an adequately complete sample. We also adopt a more simplistic approach, determining the space density of all clusters for which we have redshifts. Although this sample is incomplete, by definition, it is strictly volume-limited (also by definition) and provides a useful lower limit to the quantities of interest.

Previous studies that have targeted clusters from available 2D catalogues have approached this problem by using appropriate cuts in richness and m_{10}. For example, the ENACS survey (Katgert et al. 1996) studied all $R > 1$ Abell clusters with $m_{10} < 16.9$. This sample is approximately volume-limited to $z \sim 0.1$, but incomplete in that it does not include all clusters with $z < 0.1$. Estimated redshifts have also been used to derive information on cosmology from analysis of the distribution of Abell clusters (e.g. Postman et al. 1985). It is therefore of interest to consider the accuracy of photometric redshift estimators via comparison with our more accurately determined 2dFGRS spectroscopic values.

4.1 The Abell/ACO sample

Fig. 5(a) plots estimated redshifts (using the formulae in Scaramella et al. 1991) versus 2dF redshifts for the Abell sample. We see an acceptable linear relationship, with some tendency to saturate at very high redshifts (where the estimated redshift is slightly higher than the measured one).
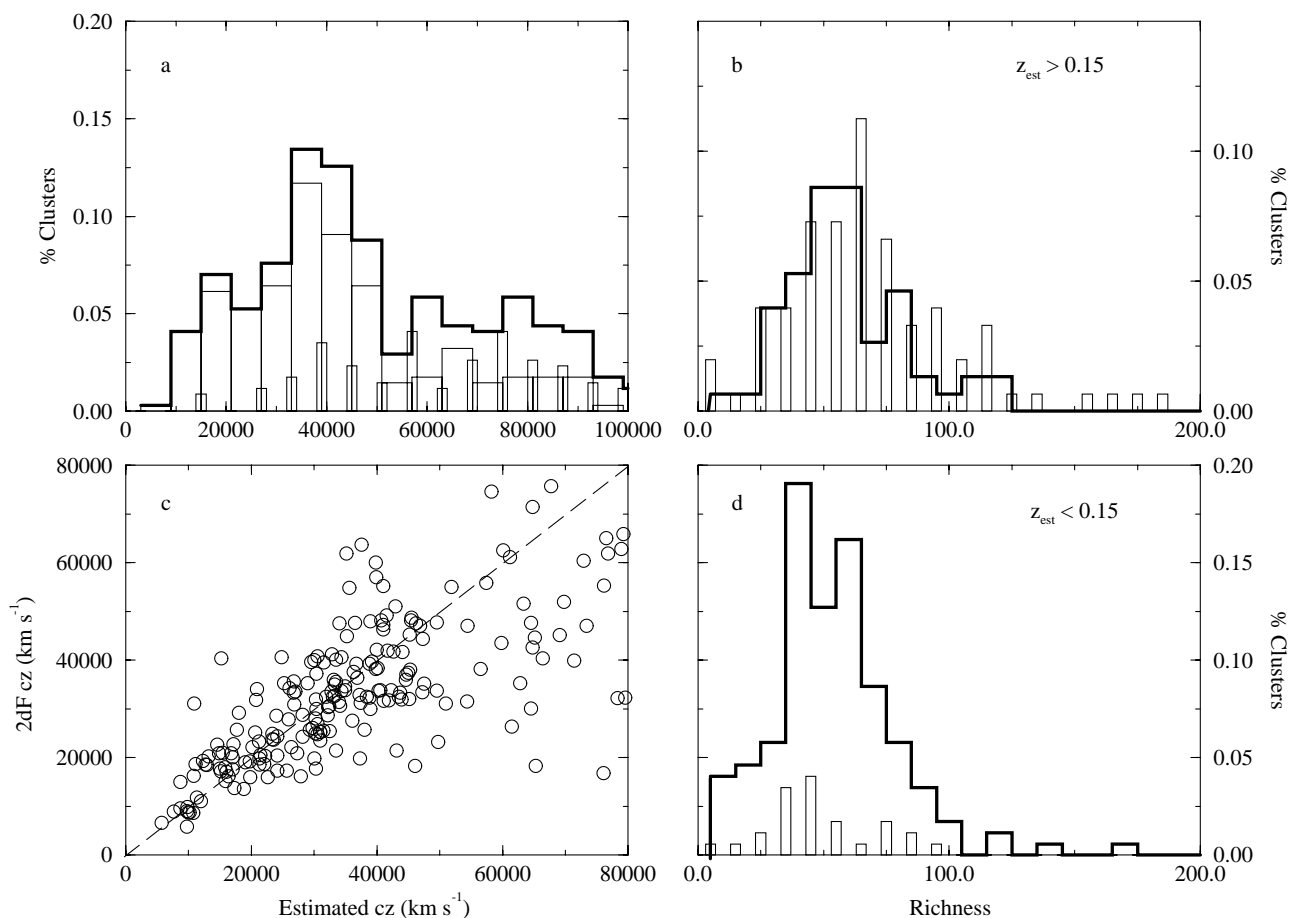
Figure 5. Data for the Abell sample. Panel (a) compares estimated and measured redshifts; panel (b) shows the fraction of clusters as a function of estimated redshift: the broad, thin-lined histogram represents the catalogued clusters, the thick-lined histogram represents the clusters identified within 2dFGRS, and the thin-lined narrow bars represent clusters that were missed. Panels (c) and (d): as for panel (b), but the fractions are plotted as a function of richness for the $z_{est} < 0.15$ and $z_{est} > 0.15$ samples, respectively; here the thick-lined histogram represents the detected clusters, while the thin-lined histogram represents the missed clusters.

Fig. 5(b) shows what fraction of the catalogued clusters are in each of the different estimated redshift bins (width $\Delta z = 0.02$), plus the fractional distributions for both those clusters identified in 2dFGRS and those that were missed. We see that our data are reasonably complete to a redshift of about ~0.10 and our completeness drops beyond that as cluster galaxies drop below the survey magnitude limit.

We split our sample at $z = 0.15$ where approximately equal numbers of objects are missed or identified, and plot the distribution of cluster richnesses (as measured from $m_3 + 2$).

For objects with $z_{est} < 0.15$, the distributions of richnesses for identified and missed objects are similar [Fig. 5c]. Surprisingly, this is also true for objects with $z_{est} > 0.15$ in Fig. 5(d). The fraction of missed objects in the $z < 0.15$ group rises rapidly in the last two redshift bins. The similar richness distributions suggest that at least some of the missed objects are really spurious superpositions. We also plot the fractions of recovered and missed clusters as a function of completeness in each tile of 2dFGRS in Fig. 6: we see no strong trend. We also divide the sample according to richness, at the median richness of the sample ($R = 50$). Although there is a small tendency for poorer clusters to be missed in low 2dF completeness regions (as one would expect), we find no strong trend in this sense. This suggests that we would be able to find the clusters, if they are real. We calculate that about 25 per cent

of clusters in the $z_{est} < 0.15$ group are missed, which would be consistent with the estimate (van Haarlem, Frenk & White 1997) that about one-third of all Abell clusters are actually superpositions of numerous small groups along the line of sight.

4.2 The APM sample

We plot the estimated versus measured redshifts for the APM sample in Fig. 7(a). The relationship is reasonably linear, but the APM estimated redshifts saturate at $z \sim 0.12$. This effect derives from the magnitude limit used in the parent galaxy catalogues, where star-galaxy separation becomes unreliable at $b_j \sim 20.5$. Fig. 7(b) shows the 2dFGRS detection success rate as a function of completeness in the 2dFGRS tile: we note that there is some tendency for APM clusters to be missed at low completeness. We plot the fractions of all catalogued clusters, those found and those missed for the APM in Fig. 7(c), and we see that whereas the sample is complete to $z < 0.07$, clusters are increasingly missed at higher redshifts. The distribution of richnesses (Fig. 7d) shows that most of the missed objects tend to be the poorer systems, as one would expect. The more homogeneous behaviour of the APM cluster catalogue (in terms of completeness as a function of redshift and richness) is probably a reflection of the more objective search algorithm used (cf. Abell's).
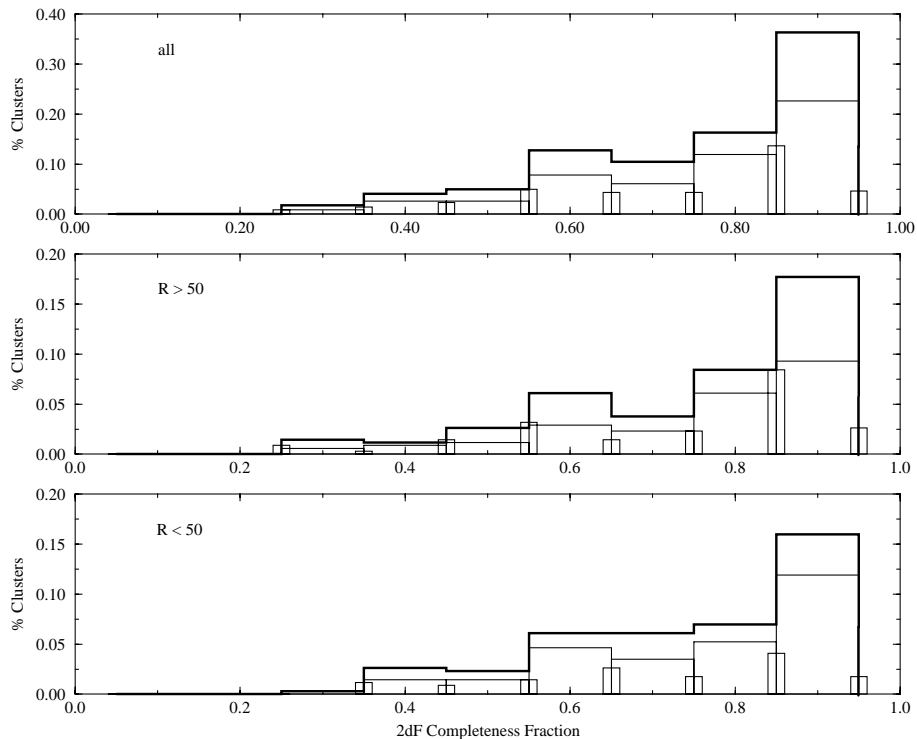
Figure 6. The same fractions as plotted in Figs. 5(b)–(d) for the sample of Abell clusters, but here plotted as a function of the redshift completeness in the 2dFGRS tile in which the cluster is located. The broad, thin-lined histogram represents the catalogued clusters, the thick-lined histogram represents the clusters identified within 2dFGRS, and the thin-lined narrow bars represent clusters that were missed. We plot all clusters in the top panel, those with $R > 50$ in the middle, and those with $R < 50$ in the bottom panel.

4.3   The EDCC sample

We plot estimated versus measured redshifts for the EDCC sample in Fig. 8(a). Here we see that EDCC tends to systematically overestimate the cluster redshift. We tried to derive a more accurate formula for EDCC estimated redshifts based on the formalism of Scaramella et al. (1991). However, we see that the m_{10} indicator for EDCC saturates quickly, and we are unable to determine a more accurate relation between estimated and true redshifts. The distribution of completeness fractions in tiles for catalogued, recovered, and missed objects are shown in panel (b), where we see a trend for clusters to be missed in low completeness regions (as one would expect). Panel (c) shows the distributions as a function of estimated redshift: here we find little difference between the three classes of clusters. Panel (d) shows the richnesses: again, recovered and missed objects follow the same distributions.

4.4   Contamination of cluster catalogues

The broad relation that exists between estimated and true redshifts has been used in previous studies to define an estimated cz such that, given the spread in the relation, the sample will be approximately volume-limited within a specified cz, although it will not necessarily be complete. We now go through this exercise here, choosing limits rather conservatively in order to minimize the level of incompleteness. By way of example, we derive 'volume-limited' cuts from estimated redshifts below, and determine the level of contamination: we also use these relationships in the next section, where we consider the space density of clusters.

For the Abell sample we choose a limit of $z < 0.11$, where our data are reasonably complete. This includes 110 clusters with 100

redshifts. Of these, nine have significant foreground or background structure. Here and for the other clusters as well, we define 'significant' to mean that we were able to derive at least a redshift, and in some cases a velocity dispersion for the background or foreground systems (these are tabulated in Table 1 as well). About 10 per cent of Abell clusters are therefore contaminated systems by our definition. If we use the original centroids, we obtain a contaminated fraction of 15 per cent. This is due to the fact that fore/background groups shift the real cluster centre away from its proper position.

For the APM catalogue we use the entire sample. Of the 173 clusters, only five are contaminated by fore/background groups, i.e., about 3 per cent. A slightly higher fraction (5 per cent) is derived from the original centroids. This lower fraction is simply due to the smaller radius used by APM, which increases the contrast between cluster and field.

The EDCC is more complicated, as the relationship between estimated and true redshifts is non-linear and shows a sizeable offset. We choose an estimated cz of $50\,000\,\mathrm{km\,s^{-1}}$ to include all objects within $30\,000\,\mathrm{km\,s^{-1}}$. This includes 234 clusters, with 165 redshifts. By our definition, 15 of these objects show contamination, equivalent to 8 per cent, similar to the Abell sample. If we adopt the original centres, we find a level of about 13 per cent contamination. This is well within the estimate by Collins et al. (1995) and is not peculiar to the EDCC catalogue, but rather an unavoidable consequence of the selection procedure imitating Abell's. The correlation results of Nichol et al. (1992) use a smaller search radius and are unaffected by the higher level of contamination.

We therefore confirm the earlier studies by Lucey (1983) and Sutherland (1988) that the Abell catalogue suffers from contamination at approximately the 15 per cent level, if the
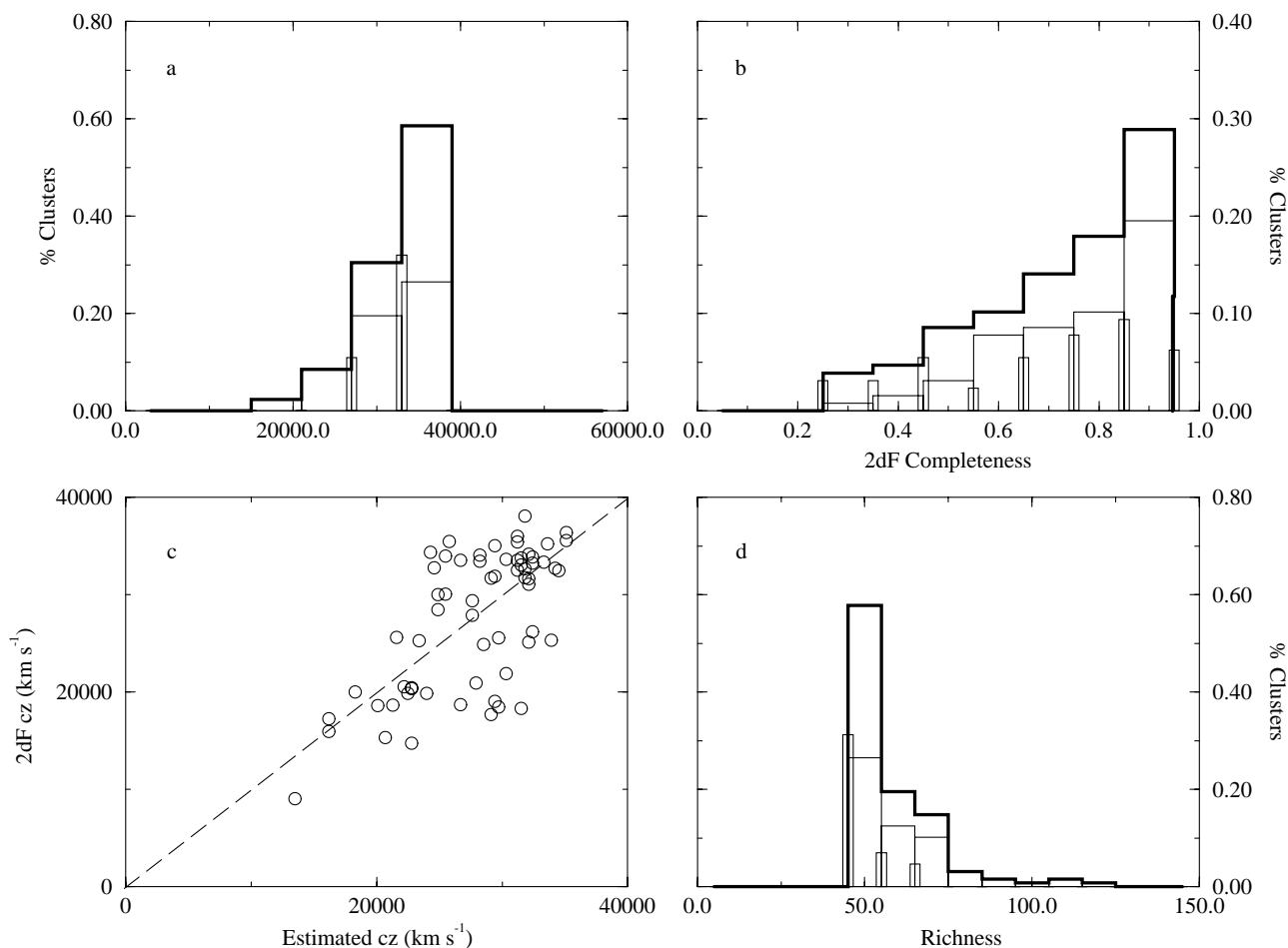
Figure 7. Data for the APM sample. Panel (a) compares estimated and measured redshifts; panel (b) shows the fraction of clusters as a function of estimated redshift: the broad, thin-lined histogram represents the catalogued clusters, the thick-lined histogram represents the clusters identified within 2dFGRS, and the thin-lined narrow bars represent clusters that were missed. Panel (c): as for panel (b), but the fractions are plotted as a function of richness; here the thick-lined histogram represents the detected clusters, while the thin-lined histogram represents the missed clusters. Panel (d): as for panel (b), but the fractions are plotted as a function of completeness in each tile.

original cluster centres are used. The EDCC catalogue behaves similarly. The APM seems to be best at selecting real clusters; this is most likely due to the smaller search radius employed by Dalton et al. (1992) and the higher richness cut used to produce the APM catalogue. If we use more accurate centres, the level of contamination is reduced, suggesting that in some cases the position and richness of the clusters are shifted by the presence of the fore/background group.

5 THE SPACE DENSITY OF CLUSTERS

We have used the 2dFGRS to select clusters over a wide range of richness and to establish a more accurate volume-limited sample than is possible from photometric indicators. Having done so, we now examine the space density of clusters as a function of redshift in each of the catalogues, in order to choose a redshift within which the sample is at least reasonably complete. The density of clusters as a function of redshift within 0.01 intervals is shown in Fig. 9. We also plot a corresponding sample from the RASS1 survey of De Grandi et al. (1999). The RASS1 is an X-ray-selected survey of Abell clusters spanning about one-third of the Southern sky: for this reason the sample is only semi-independent from ours, although it does not fully overlap with our slices. Since the true

space density of clusters is expected to be approximately constant over this range of redshifts, the observed general decline in the cluster space density at $z \geq 0.1$ must reflect the incompletenesss of the Abell, APM and EDCC catalogues at these limits (plus our own inability to detect clusters as some complex function of richness, distance and incompleteness).

Within $z < 0.15$ (chosen as the redshift range in which we are nearly complete), we see in Fig. 9 that there is considerable fluctuation of the space density. Furthermore, the Abell et al. and EDCC clusters both exhibit a density minimum at $z \sim 0.05$ (as also seen in the galaxy distribution; Cross et al. 2001) at approximately the 2σ level. The deficit extends across the entire Southern strip of the survey and possibly beyond, corresponding to a $200 \, \mathrm{Mpc} \, h^{-1}$ scale void. While this is potentially very interesting, we must be extremely cautious at this stage that this is not just a sampling effect that results from the small (and hence unrepresentative) volume so far covered by the 2dFGRS at these low redshifts. We note that a similar effect has been noted by Zucca et al. (1997) in the ESO slice survey (ESP), and can be explained in the same manner if one considers the location of the ESP within the APM Galaxy Survey map. A comparison with the wider RASS1 survey of X-ray-selected clusters, also plotted in Fig. 7, shows no evidence of such a structure.
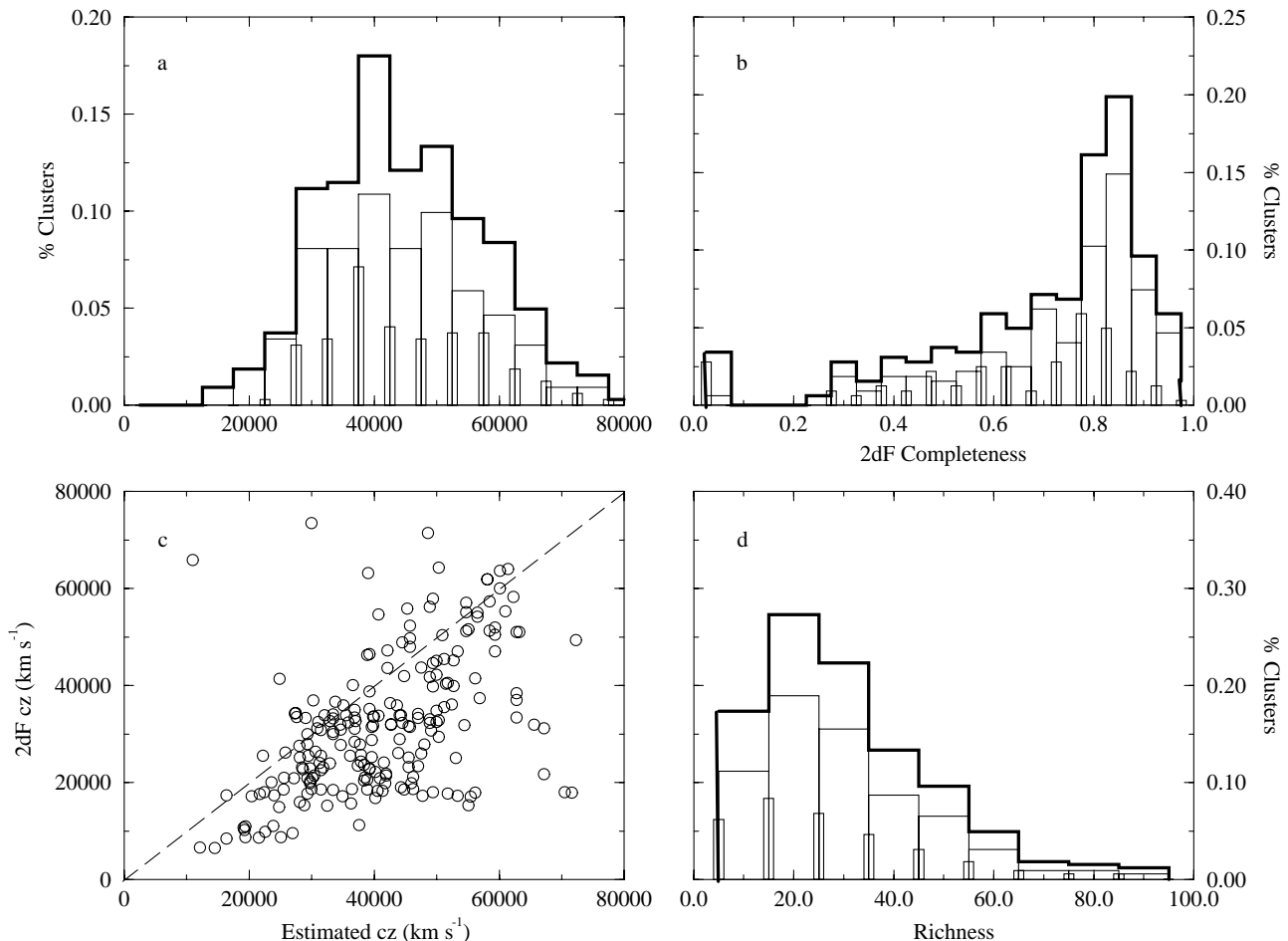
Figure 8. As per Fig. 6 for the EDCC clusters.

However, three semi-independent samples show this feature at statistically significant levels. It would be difficult to devise a selection effect working against $z \sim 0.05$ clusters (only) in a 2D sample. Subject to the caveats above, these data are suggestive of a large underdensity in the Southern hemisphere, in the direction sampled by the APM. This would account for the low normalization of the bright APM counts without requiring strong evolution at low redshift (Maddox et al. 1990c) and for the differences in the amplitude of the ESP and Loveday et al. (1992) field luminosity functions. This deficit is not seen in some other surveys because of the Shapley concentration, which masks the underdensity centred close to the South Galactic Pole. For instance, the REFLEX survey reports an overdensity at this redshift which is attributed to the Shapley structure (Schuecker et al. 2001).

In order to derive the distribution of cluster velocity dispersions to be discussed in the next section, we need to determine the *true* space density of catalogued Abell clusters. Naturally, this is but a lower limit to the space density of *all* clusters, which can only be derived from a 3D-selected sample, but, at least for the richer clusters, our sample should be complete. We restrict our attention to Abell clusters, which are the most commonly used sample of objects.

As we have seen, it is possible to use the linear relationship between estimated and true redshifts for the Abell sample to define a reasonably complete sample to $z \sim 0.11$. In the two survey strips we have surveyed a total of 984.8 square degrees. We therefore derive a space density of $(27.8 \pm 2.8) \times 10^{-6} \, h^3 \, \mathrm{Mpc}^{-3}$ for all

Abell clusters, and $(9.0 \pm 1.7) \times 10^{-6} \, h^3 \, \mathrm{Mpc}^{-3}$ for clusters of richness class 1 or greater. In comparison, Scaramella et al. (1991) derive a space density of about $6 \times 10^{-6} \, h^3 \, \mathrm{Mpc}^{-3}$, and Mazure et al. (1996; ENACS) obtain 8.6×10^{-6}. Our result is in good agreement with the ENACS value, but somewhat higher than that of Scaramella et al.

6 VELOCITY DISPERSION DISTRIBUTION

The cumulative distribution of velocity dispersions provides constraints on cosmological models of structure formation, via the shape of the power spectrum of fluctuations. The power spectrum at large scales can be determined from the *COBE* data (and subsequent cosmic microwave background experiments), whereas cluster mass functions yield limits on small scales. Although it is generally difficult to estimate cluster masses, the distribution of velocity dispersions may be used as a substitute. In particular, the space density of the most massive (high-σ) clusters is a good discriminant between theoretical models.

We assume that the distribution of velocity dispersions for clusters with $z < 0.11$ represents the underlying true distribution. Some support for this is given by Fig. 10, where we plot velocity dispersion versus redshift and find no obvious correlation. This suggests that our sample is 'fair' in the sense that we are not systematically losing clusters at any particular velocity dispersion.

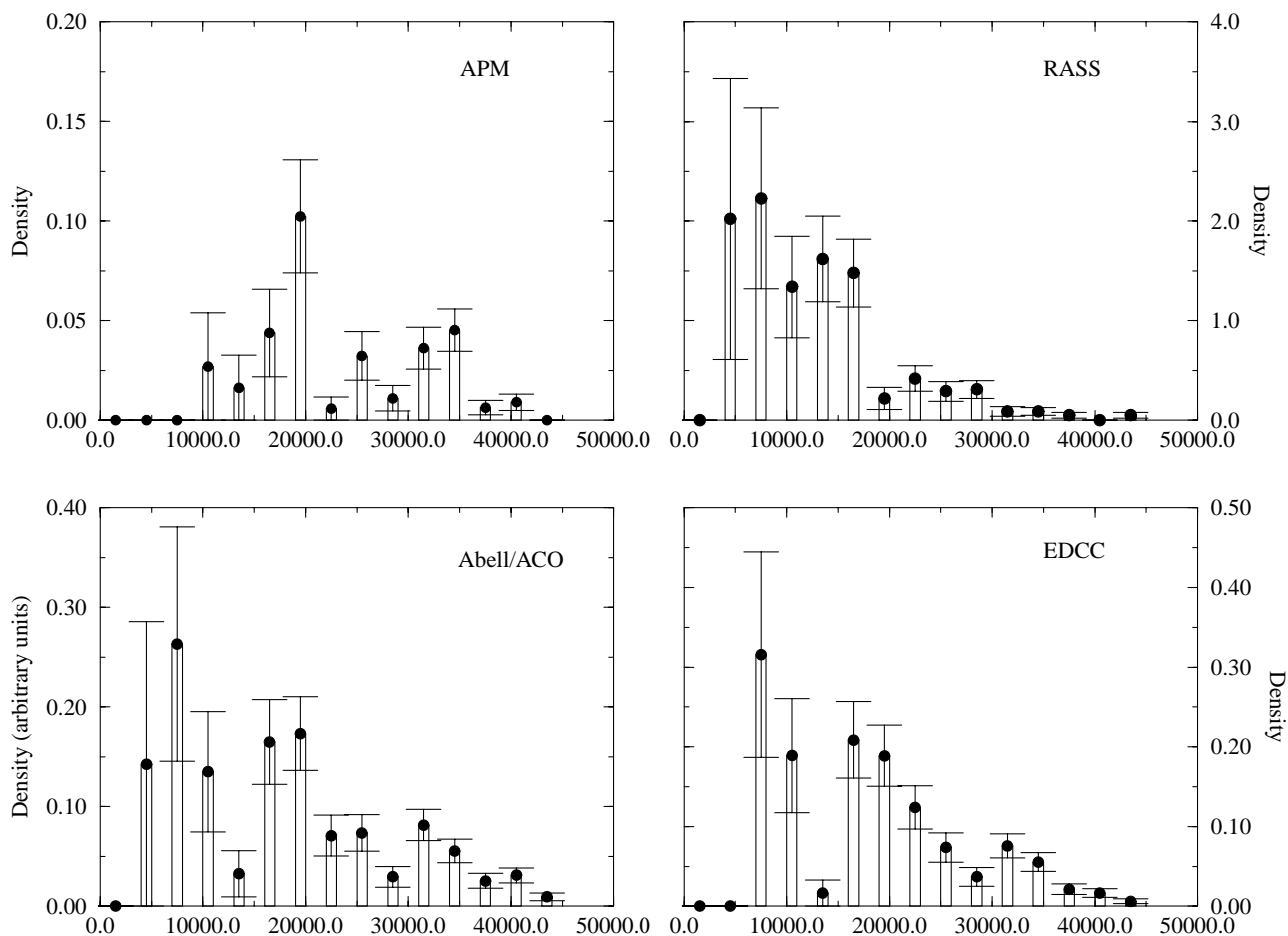We plot our data in Fig. 11 (filled circles), together with previous

Figure 9. Variation of space density (normalized to volume) for Abell, APM and EDCC clusters and the RASS1 sample. Units of density are arbitrary.

work by Girardi et al. (1993), Zabludoff et al. (1993) and Mazure et al. (1996) (all as lines). For the sake of comparison, we renormalize these data to our local density. These should be taken with some caution, especially at low velocity dispersions, where our sample includes low-richness objects (and all the samples become incomplete at some level), but should be reasonable at high velocity dispersions, where our results are in acceptable agreement with previous data.

The most robust result of our analysis is the confirmation of a relative lack of high-σ clusters. As a matter of fact, since interloper galaxies cause a spurious high-σ tail in the distribution (van Haarlem et al. 1997), we feel we can derive a significant value to the space density of $N(\sigma > 1000\,\mathrm{km\,s^{-1}})$ clusters. We consider only clusters whose *derived* redshifts place them within $z < 0.11$. This is equivalent to $(3.6 \pm 1) \times 10^{-6}\,h^3\,\mathrm{Mpc^{-3}}$ and may be compared with theoretical models by Borgani et al (1997), for instance: our data are in good agreement with a cold+hot dark matter model; a ΛCDM model with $\Omega_M = 0.3$ underpredicts the space density of clusters whereas one with $\Omega_M = 0.5$ slightly overpredicts it; τCDM models are acceptable as long as $\sigma_8 < 0.67$; open CDM models with $\Omega_M = 0.6$ are in good agreement with our results, and standard CDM models normalized to *COBE* (as are all models in Borgani et al.) are inconsistent with our derived space density. The data therefore favour low matter densities or small values of σ_8 (where σ_8 is the rms fluctuation within a top-hat sphere of $8\,h^{-1}\,\mathrm{Mpc}$ radius). This would bring cluster results into better agreement with the *COBE* data (e.g. Bond & Jaffe 1999).

7 SUMMARY

We have analysed a sample of 1149 previously catalogued clusters of galaxies that lie within the 2dFGRS. The results of this analysis can be summarized as follows.

(1) New redshifts (and velocity dispersions) have been derived for a sample of 263 (208) clusters in the Abell sample, 84 (75) APM clusters and 224 (174) EDCC clusters.

(2) Of the 1149 clusters, 753 appear to have no counterpart in each of the other catalogues and are thus unique.

(3) The level of contamination of our clusters by fore/background groups is about 10 per cent for the Abell sample. However, if we select on the original centroids, we confirm the earlier results of Lucey (1983) and Sutherland (1988) that for about 15–20 per cent of the Abell and EDCC clusters, background and foreground groups substantially boost the derived surface density and may lead to poor groups being erroneously identified as clusters. This shows that the presence of interloper groups and galaxies may skew the apparent richness and structure of clusters.

(4) The space density of rich Abell clusters is broadly consistent with previous work. For all Abell clusters the derived space density is $(27.8 \pm 2.8) \times 10^{-6}\,h^3\,\mathrm{Mpc^{-3}}$; for $R > 1$ clusters, we find a space density of $(9.0 \pm 1.7) \times 10^{-6}\,h^3\,\mathrm{Mpc^{-3}}$. This is broadly consistent with, but better determined than, previous work.

(5) We find evidence for the existence of an underdensity of clusters in the Southern hemisphere at $z \sim 0.05$.
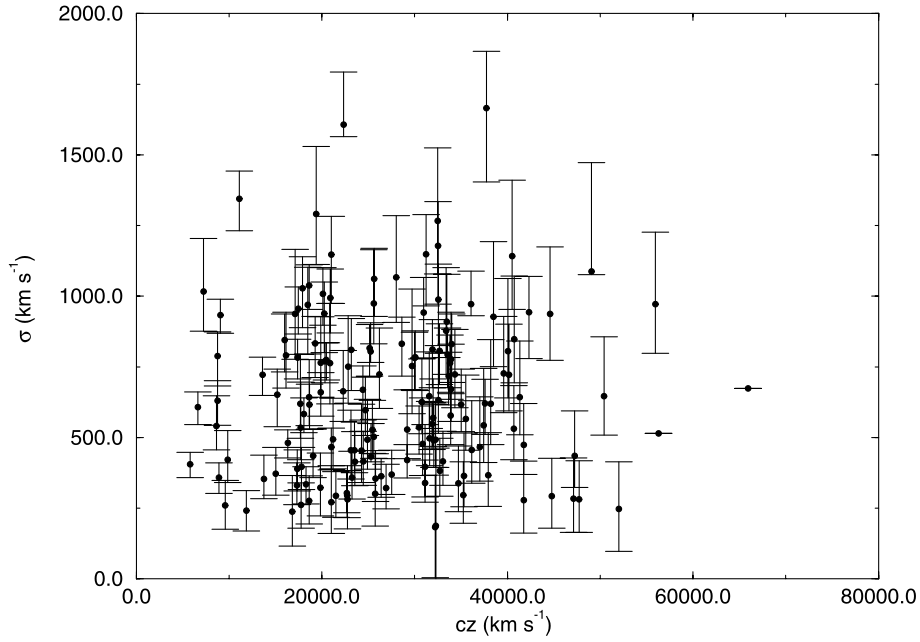
Figure 10. Derived velocity dispersion versus redshift for the Abell sample, showing the lack of correlation.
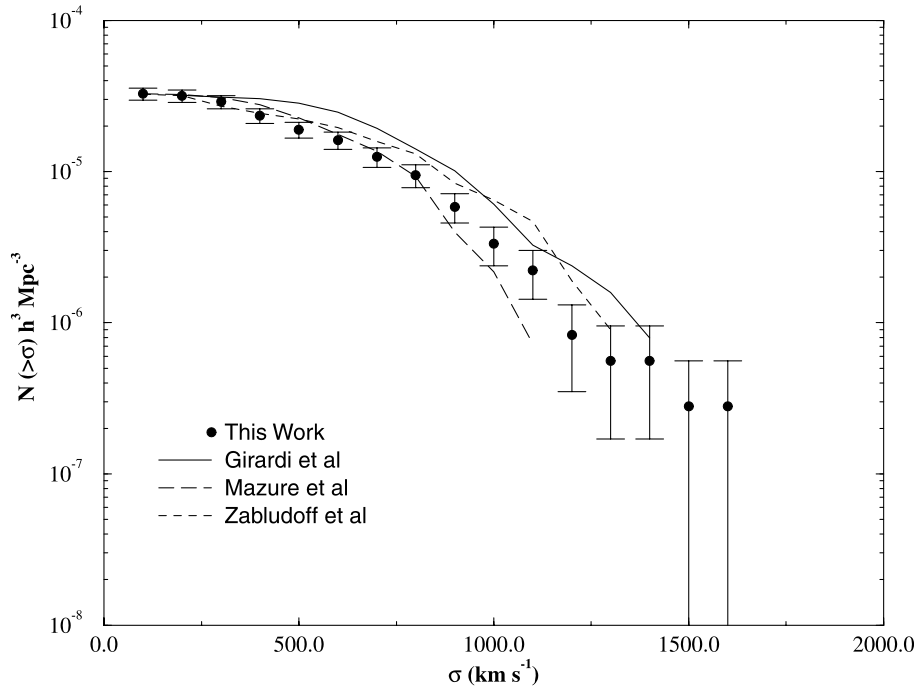

Figure 11. Distribution of velocity dispersions for our sample and previous work. We have renormalized Girardi et al. and Mazure et al. data for the sake of comparison.

(6) We derive an upper limit to the space density of clusters with velocity dispersion greater than $1000\,\mathrm{km\,s}^{-1}$. This is shown to be inconsistent with some models of structure formation, and to favour generally low matter densities and low values of the σ_8 parameter.

REFERENCES

Abell G. O., 1958, ApJS, 3, 211
Abell G. O., Corwin H. G., Olowin R., 1989, ApJS, 70, 1 (ACO)

Beers T. C., Flynn K., Gebhardt K., 1990, AJ, 100, 32

Bond J. R., Jaffe A. H., 1999, Phil. Trans. Roy. Soc., 357, 57

Borgani S., Gardini A., Girardi M., Gottlöber S., 1997, New Astronomy, 2, 199

Colberg J. M. et al., 1998, in Hamilton D., ed., The Evolving Universe: Selected Topics on Large Scale Structure and on the Properties of Galaxies, Astrophysics and Space Science Library, 231. Kluwer, Dordrecht, p. 389

Colless M., 1998, in Colombi S., Mellier Y., Raban B., eds, Wide Field Surveys in Cosmology. Editions Frontieres, Paris, p. 77

Colless M. et al., 2001, MNRAS, in press

Collins C. A., Guzzo L., Nichol R. C., Lumsden S. L., 1995, MNRAS, 274, 1071

Crone M. M., Geller M., 1995, AJ, 110, 21

Cross N. D. et al., 2001, MNRAS, 324, 825

Dalton G. B., Efstathiou G., Maddox S. J., Sutherland W. J., 1992, ApJ, 390, L1

Dalton G. B., Maddox S. J., Sutherland W. J., Efstathiou G., 1997, MNRAS, 289, 263

Danese L., de Zotti G., di Tullio G., 1980, A&A, 82, 322

De Grandi S. et al., 1999, ApJ, 514, 148

Dubinski J., 1998, ApJ, 502, 141

Girardi M., Biviano A., Giuricin G., Mardirossian F., Mezzetti M., 1993, ApJ, 404, 38

Katgert P. et al., 1996, A&A, 310, 8

Loveday J., Peterson B. A., Efstathiou G., Maddox S. J., 1992, ApJ, 390, 338

Lucey J. R., 1983, MNRAS, 204, 33

Lumsden S. L., Nichol R. C., Collins C. A., Guzzo L., 1992, MNRAS, 258, 1

Maddox S. J., Efstathiou G., Sutherland W. J., Loveday J., 1990a, MNRAS, 243, 692

Maddox S. J., Efstathiou G., Sutherland W. J., 1990b, MNRAS, 246, 433

Maddox S. J., Sutherland W. J., Efstathiou G., Loveday J., Peterson B. A., 1990c, MNRAS, 247, 1P

Maddox S. J. et al., 1998, in Müller V., Gottlöber S. G., Mücket J. P., Wambsganss J., eds, Large Scale Structure: Tracks and Traces. World Scientific Singapore, Singapore, p. 91

Mazure A. et al., 1996, A&A, 310, 31

Nichol R. C., Collins C. A., Guzzo L., Lumsden S. L., 1992, MNRAS, 255, 21P

Postman M., Huchra J. P., Geller M., Henry J. P., 1985, AJ, 90, 1400

Scaramella R., Zamorani G., Vettolani G., Chincarini G., 1991, AJ, 101, 342

Schuecker P. et al., 2001, A&A, 368, 86

Scott E. L., 1956, AJ, 61, 190

Shectman S. A., 1985, ApJS, 57, 77

Struble M. F., Rood H. J., 1999, ApJS, 125, 35

Sutherland W., 1988, MNRAS, 234, 159

Sutherland W., Efstathiou G., 1991, MNRAS, 248, 159

van Haarlem M. P., Frenk C. S., White S. D. M., 1997, MNRAS, 287, 817

Yahil A., Vidal N. V., 1977, ApJ, 214, 347

Zabludoff A. I., Huchra J. P., Geller M. J., 1990, ApJS, 74, 1 (ZHG)

Zabludoff A. I., Geller M. J., Huchra J. P., Ramella M., 1993, AJ, 106, 1301

Zucca E. et al., 1997, A&A, 326, 477

This paper has been typeset from a TEX/LATEX file prepared by the author.